Available online at www.sciencedirect.com

ScienceDirect

Procedia Engineering 2 (2010) 1045–1056

Procedia Engineering

www.elsevier.com/locate/procedia

Fatigue 2010

Simulation-based extreme value marked correlations in fatigue of advanced engineering alloys

Craig P. Przybyla[*,a,b] , David L. McDowell[b,c]

[a]*Materials and Manufacturing Directorate, AFRL, Wright-Patterson AFB, OH, 45433, USA*
[b]*School of Materials Science an d Engineering, Georgia Tech, Atlanta, GA, 30332, USA*
[c]*GWW School of Mechanical Engineering, Georgia Tech, Atlanta, GA, 30332, USA.*

Received 20 February 2010; revised 10 March 2010; accepted 15 March 2010

Abstract

The objective of this research is to estimate the microstructure dependence of the extreme value probabilities of fatigue crack formation at the scale of the grains in polycrystalline and polyphase microstructures to facilitate preliminary parametric design exploration and property assessment. A simulation-based methodology is introduced for computing correlation functions of microstructure attributes marked by the extreme value microstructure-scale fatigue indicator parameters. Multiple statistically representative microstructure volumes simulated using a crystal plasticity constitutive model coupled with the FEM are used to characterize these extreme value marked correlation functions. By comparing these marked correlation functions to traditional correlation functions sampled from the bulk material, the interacting microstructure attributes important to the extreme value response are identified. This methodology is applied to identify dominant crystallographic relationships relative to fatigue crack formation in the polycrystalline P/M Ni-base superalloy IN100 and duplex Ti-6Al-4V. It is demonstrated that certain high contrast orientation relationships in both IN100 and Ti-6Al-4V (where grains oriented for hard slip are near grains oriented for easier slip) can significantly increase the driving forces for fatigue crack formation.

Keywords: metal fatigue; extreme value statistics; marked correlation functions; microstructure-sensitive design; Ni-base superalloys; Ti-6Al-4V.

1. Introduction

Component service life under cyclic loading is primarily a function of the extreme value probabilities of life limiting microstructure attributes or combinations of microstructure attributes. The life limiting microstructure attributes are those that increase the driving forces for fatigue crack formation the most within a given volume of material. Moreover, multiple interacting microstructure attributes that exist together with varying probabilities can further enhance local driving forces for fatigue crack formation. Traditionally, the extreme value microstructure dependence of components subjected to cyclic loads has only been captured empirically through extensive experimentation. In the last few decades, much work has been done to better understand the microstructure dependent mechanisms of fatigue crack formation in metals [1, 2]. However, to predict variability of fatigue crack

[*] Corresponding author. *E-mail address*: craig.przybyla@wpafb.af.mil

1877-7058
doi:10.1016/j.proeng.2010.03.113

formation, a framework is needed that accounts for the extreme value life limiting attributes most relevant to the processes of fatigue crack formation.

Current probabilistic approaches that account for the extreme value statistics of life limiting microstructure attributes relative to fatigue crack formation consider only distributions of a single microstructure attribute and do not account for the effect that multiple interacting microstructure attributes has on the extreme value response distributions. For example, Murakami *et al.* [3, 4] use classical extreme value Gumbel statistics to estimate the size of the largest inclusion based on specimen volume. In this case, the authors use extreme value statistics of inclusion size to estimate the fatigue strength in clean steels based on the assumption that the life limiting fatigue crack tends to form at the largest inclusion within a given volume,. Similarly, Atkinson and Shi [5] use a generalized Pareto distribution to estimate the size of the largest inclusion for a given volume. The difference being that the generalized Pareto distribution incorporates a limit on the maximum inclusion size; whereas, the extreme value Gumbel distribution predicts an ever increasing inclusion size for increasing volumes. These types of models based on a single microstructure attribute like inclusion size do not account for interactions between the inclusion and surrounding matrix, for example. Although first order approaches based on single microstructure attributes may suffice for some material systems or applications, fatigue crack formation in many advanced engineering alloys can be very complex. As such, to understand the processes of fatigue crack formation in complex material systems, a better probabilistic description of the interactions between multiple microstructure attributes is required.

The objective of this research is to apply a newly developed extreme value microstructure sensitive probabilistic framework to quantify the influence of polycrystalline microstructure on fatigue crack formation in the polycrystalline P/M Ni-base superalloy IN100 and in duplex Ti-6Al-4V under HCF conditions. Specifically, this new probabilistic framework uses extreme value marked correlation functions for microstructure attributes to quantify the interacting microstructure attributes that are most statistically significant relative to the measured or simulated extreme value distributions of response [6, 7]. Correlation functions for the microstructure attributes important to the operant mechanisms of fatigue crack formation are selectively sampled in regions marked by certain extreme value response parameters (*e.g.* cyclic plastic strain range). These extreme value marked correlations can then be compared to the same correlation functions sampled over the entire microstructure ensemble (i.e., without regard to response) to determine the particular correlated microstructure attributes that are most significant. In general, this methodology can be applied to quantify important correlated microstructure attributes relative to their influence on the extreme value distributions of response for many different damage processes (e.g. fatigue, creep, fracture). In this work, multiple material volumes for both IN100 and Ti-6Al-4V are simulated via the FEM with crystal plasticity constitutive relations to explore how local crystallography influences the distributions of the estimated driving forces for fatigue crack formation as estimated by certain cyclic plasticity based fatigue indicator parameters (FIP).

1.1. Fatigue crack formation in polycrystalline P/M Ni-base superalloy IN100

Typically, fatigue damage formation in polycrystalline superalloys has been linked to the existence of large pores or nonmetallic inclusions introduced during processing. Fatigue cracks form at inclusions/pores under cyclic loading because of local stress concentrations [8-10]. In some cases, however, cleaner polycrystalline Ni-base superalloys are being developed that exhibit fatigue crack formation along crystallographic planes in samples or components absent of inclusions/pores. For example, Jha *et al.* [11] noted that subsurface fatigue crack formation occurs in individual grains absent of any voids/inclusions in René 88DT in the HCF regime at 593°C. Here the crystallographic facets associated with fatigue crack formation were observed to be much larger than the average grain size, suggesting that cracks tend to form in larger grains. Similar results were reported by Miao *et al.* [12] in the same superalloy in the VHCF regime. In particular, Miao *et al.* noted that the faceted grains near the fatigue crack formation site were associated with large grains, higher Schmid factors for {111}<110> slip and twin boundaries of a particular character.

Different slip modes appear to be more important depending on the service temperature. The γ austenitic phase in Ni-base superalloys has a fcc crystalline lattice, which has 12 octahedral {111}<110> slip systems. Moreover, at elevated temperatures apparent effects of an additional 6 cube {100}<110> slip systems have been observed in the γ phase in many Ni-base superalloys in the form of macroscopic slip traces [13]. Although limited cube slip is possible in the Ll_2 ordered γ' phase, it is not commonly considered as likely to occur in the austenitic γ phase. Based

on observations via transmission electron microscopy (TEM), Bettge and Österle [13], postulated that cube slip traces observed along {100} *planes* is due to "zig-zag" cross slip of screw dislocations on {111} planes within channels between γ' precipitates. In polycrystalline P/M Ni-base superalloy IN100, fatigue cracks have been observed to propagate along {111} planes at lower homologous temperatures and along {100} planes at moderate temperatures (e.g., between 500°C to 800°C) [14].

1.2. Fatigue crack formation in α+β Ti alloys

Fatigue crack formation in $\alpha+\beta$ Ti alloys is primarily associated with the development of crystallographic facets at the grain scale. Bridier *et al.* [15, 16] investigated fatigue crack formation in Ti-6Al-4V in both LCF and HCF, respectively, and found that cracks primarily form on basal slip planes (particularly those with somewhat elevated level of peak normal stress to the basal plane) and less frequently on prismatic slip planes favorably oriented for slip. Gilbert and Piehler [17] observed internal fatigue crack formation on pyramidal planes in the primary α grains in Ti-6Al-4V oriented for hard basal slip (i.e., with c axis nearly parallel to the loading direction). Clusters of grains oriented for slip on pyramidal $<a+c>$ planes and grains oriented for basal slip were observed by the authors to enhance fatigue crack formation. Szczepanski *et al.* [18] observed fatigue facet formation in the VHCF regime of Ti-6246 on or near basal or prismatic slip planes favorably oriented for slip. In the same material, Jha and Larsen [19] noted that at moderate stress amplitudes (i.e., close to the macroscopic yield stress) that facets near the location of initial fatigue crack formation were all inclined ~35-45° relative to the loading axis. In one sample, the facet near the location of initial fatigue crack formation appeared to be ~35° relative to the loading direction in a grain oriented unfavorably for basal slip, suggesting the facet was formed by a $<c+a>$ hard slip mechanism (i.e., pyramidal slip). In another sample, the facet near the location of initial fatigue crack formation developed on an apparent basal slip plane favorably oriented for slip. The grain unfavorably oriented for basal slip that developed the facet was surrounded by other grains more favorably oriented for easy slip (i.e., prismatic or basal slip). Additionally, the sample with the facet that formed in the grain oriented for hard basal slip failed at ~60,000 cycles; whereas, in the other sample with the facet that formed in the grain oriented for easy basal slip failed at ~2,000,000 cycles.

1.3. Fatigue indicator parameters

Simulation-based strategies for investigating microstructure-resolved driving forces for fatigue crack formation have greatly expanded in recent years. McDowell [20] outlined the use of plastic shear strain- based FIPs to estimate the driving forces for fatigue crack formation in metals due to plastic ratcheting and reversed cyclic plasticity. For example, the maximum plastic shear strain range (MPSS) and Fatemi-Socie (FS) [21] FIPs, i.e.,

$$P_{MRSS} = \frac{\left\langle \Delta\gamma^{p}_{\max} \right\rangle_{V}}{2} \tag{1}$$

and

$$P_{FS} = \frac{\left\langle \Delta\gamma^{p}_{\max} \right\rangle_{V}}{2}\left(1 + K\frac{\sigma^{n}_{\max}}{\sigma_{y}}\right) \tag{2}$$

are functions of the maximum plastic shear strain range $\left\langle \Delta\gamma^{p}_{\max} \right\rangle_{V}$. The stress normal to the plane of maximum plastic shear is given by $\sigma^{n}_{\max}$, σ_y is macroscopic cyclic yield stress, and K controls the effect of the normal stress on fatigue crack formation. Calculations of the FS FIP for both IN100 and Ti-6Al-4V are carried out with a value of K=1 based on previous studies (*e.g.* [7]). Volume averaging over scales pertinent to the microstructure attributes relevant the processes of fatigue crack formation is indicated by the notation $<*>_V$.

These types of FIPs have been used to investigate the influence of several different microstructure attributes relative to their potency for fatigue crack formation. In martensitic gear steels, Prasannavenkatesan *et al.* [22] used these two parameters to characterize the relative potency of different kinds of inclusions to form grain/inclusion scale HCF cracks. Similar FIPs have also been used to characterize the influence of microstructure on fatigue crack formation in structural steel [23, 24] and Ni-base superalloys [6, 7, 25-27]. These efforts have demonstrated the utility in using these types of parameters coupled with crystal plasticity simulations to correlate microstructure scale

slip with fatigue crack formation and early stages of microstructurally small crack growth, particularly for purposes of comparing relative fatigue resistance of different microstructure morphologies.

2. Methodology

2.1. Extreme value marked correlation functions

A novel microstructure-sensitive extreme value probabilistic framework has recently been proposed that links correlated microstructure attributes to extreme value response via extreme value marked correlation functions [6, 7]. To construct the extreme value marked correlation functions, one must first construct the extreme value distributions of the response parameter of interest (*e.g.*, stress, strain, plastic strain). Based on classical extreme value probability theory (*cf.* [28]), the probability distribution of the extreme valued response parameter α (*e.g.*, $\alpha \equiv$FIP) is defined as $F^{ex}(\alpha|\Omega)$ given a window Ω. Thus, $F^{ex}(\alpha|\Omega)$ describes the probability that the response parameter of value α is the extreme value for a sampled volume of microstructure Ω. The extreme value marked radial correlation function as $R^{\max(\alpha)}(\beta,\beta'|r,\Omega)dr$, is defined as the probability that a microstructure attribute β located coincident with the extreme value response parameter α in Ω is located within a distance of r to $r + dr$ of a second microstructure attribute β' in any direction. We can similarly define an extreme value marked n-point correlation function, extreme value marked lineal path correlation function, extreme value marked nearest neighbor correlation function, etc. [29]. The extreme value response distribution functions describe the extreme value response of the microstructure as represented by the response parameter α. Coupled with extreme value response distribution, the extreme value marked correlation functions then describes the probabilities of existing correlated microstructure attributes, β and β', relative to the observed extreme values of α in a microstructure window Ω. Comparing $R^{\max(\alpha)}(\beta,\beta'|r,\Omega)dr$ to the correlation function for the same microstructure attributes sampled from the complete material ensemble (*e.g.*, bulk) or $R(\beta,\beta'|r)dr$, the correlated microstructure attributes most unique to the locations of extreme value response can be identified.

2.2. Simulated statistical volume elements

To characterize the microstructure attributes most important to the slip-dominated processes of fatigue crack formation in HCF in IN100 and Ti-6Al-4V, here we consider the crystallographic attributes of the microstructure (*e.g.*, phase, grain orientation, grain disorientation, grain size, and grain shape distributions). In IN100, we recognize that fatigue crack formation is most influenced by the presence of non-metallic inclusions and/or pores. However, Ni-base superalloys have been developed with much smaller populations of these types of inclusions/voids that fail crystallographically (*e.g.*, [30]). Thus, here we consider how this variant of IN100 would fail crystallographically in the absence of non-metallic inclusions or voids. In the case of Ti-6Al-4V, fatigue crack formation is predominantly crystallographic and is very much influenced by the microstructure attributes being considered here. The driving forces for fatigue damage formation on the scale of the grains are estimated by the MPSS and the FS FIPs introduced previously. In each microstructure, these parameters are averaged over volumes corresponding to grain size.

To construct the extreme value marked correlation functions, multiple simulated statistical volume elements (SVE) or microstructure instantiations (i.e., microstructure window Ω) were constructed for both IN100 and Ti-6Al-4V in the form of meshed polycrystalline microstructures with explicit grains and phases. Using the FEM, variations in local crystallographic response can be simulated using crystal plasticity constitutive relations. Each SVE is constructed based on predefined distributions of grain size, grain orientation, and grain misorientation. Here we define a SVE based on the local plastic response. In other words, each SVE is constructed to be large enough such that the local plastic strain (on the scale of the grains) is unaffected by statistical variations in the microstructure at distances on the order of the size of the SVE [7].

The SVEs for IN100 were constructed based on a Voronoi tessellation algorithm that optimized the microstructure to fit a predefine grain size distribution via a simulated annealing algorithm [7]. The duplex Ti-6Al-4V SVEs were generated using an ellipsoidal based microstructure generator. This method uses known distributions of the aspect ratios of grain equivalent ellipsoids fit to grains of experimentally characterized microstructures. Using grain equivalent ellipsoids instead of other space filling methods like Voronoi tessellation allows construction of

more complex grain morphologies such as elongated grains common in rolled ductile metals. For example, Brahme *et al.* [31] used ellipsoids fit to actual grain distributions to reconstruct Al microstructures with elongated grains. Groeber *et al.* has used similar methods to reconstruct polycrystalline representations of IN100 characterized from three-dimensional serial sections [32, 33]. The ellipsoid packing based digital microstructure generation algorithm was implemented in MATLAB [34], with logic as follows:

1. An ellipsoid is generated by randomly selecting the ellipsoid aspect ratios from a predefined distribution (*e.g.*, beta distribution).
2. The orientation of the ellipse is randomly selected based on a predefined distribution (i.e., orientation distribution function for orientation of major axes of grain equivalent ellipsoids relative to the specimen axis).
3. The ellipsoid is randomly placed in the volume. If the ellipsoid overlaps with any previously placed ellipsoid, a new random location is selected repeatedly until no overlap exists.
4. Steps 1 through 4 are repeated until the jamming limit is reached and no more non-overlapping ellipsoids can be placed in the volume.
5. The ellipsoids are then allowed to grow uniformly until all the space in the microstructure volume is filled.

A two-dimensional section of a generated microstructure using this method with a bi-modal grain size distribution is given in Figure 1. The target and generated bimodal grain size distribution of a SVE for Ti-6Al-4V is given in Figure 2.

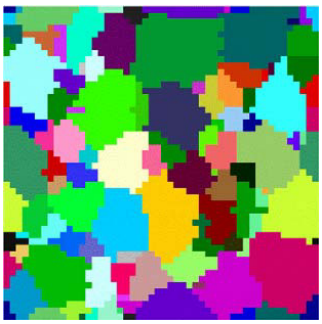

Figure 1 2-D section of a microstructure generated using the ellipsoid packing algorithm with a bi-modal grain size distribution.

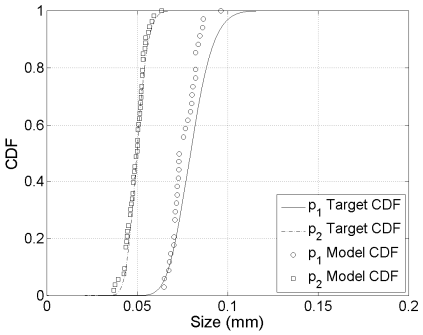

Figure 2 Target log-normal and fit model distributions of the grain size for the primary α grains and the α+β.

The crystal plasticity constitutive model for IN100 was developed by Shenoy *et al.* [35, 36]. This model does not explicitly model the γ' precipitates, but accounts for the influence of the primary, secondary and tertiary γ' precipitates via certain internal state variables incorporated into specific hardening laws. This model also accounts for the average effect of the grain size on the constitutive response and the dependence of the flow stress on crystallographic orientation. Shenoy *et al.* [35, 36] considers both the standard 12 octahedral <110>{111} slip systems and 6 cube slip systems {100}<110>. This crystal plasticity model for IN100 was calibrated at 650°C and incorporated into a User MATerial Subroutine (UMAT) for use in the commercially available FE package ABAQUS [37].

The crystal plasticity model for Ti-6Al-4V was developed by Bridier *et al.* [38] for application to the HCF loading regime for peak stresses at or below the macroscopic yield strength. The model accounts for four different families of slip systems in the primary α phase: three $<11\bar{2}0>\{0001\}$ basal, three $<11\bar{2}0>\{10\bar{1}0\}$ prismatic, six $<11\bar{2}0>\{10\bar{1}1\}$ first order pyramidal $<a>$ and twelve $<11\bar{2}3>\{10\bar{1}1\}$ first order pyramidal $<a+c>$ slip systems or a total of 24 possible modes of slip. However, slip is dominant in the basal and prismatic slip systems due to a relatively low critical resolved shear stress when compared to the other slip systems. The lamellar $\alpha+\beta$ colonies are homogenized in this model. A crystallographic burgers orientation relation (BOR) is maintained between the secondary α and β laths defined such that $(0001)_\alpha$ // $\{101\}_\beta$ and $<0001>_\alpha$ // $\{111\}_\beta$. The 24 possible slip systems

in the lamellar region include three $<11\bar{2}0>\{0001\}$ basal, three $<11\bar{2}0>\{10\bar{1}0\}$ prismatic, six $<11\bar{2}0>\{10\bar{1}1\}$ first-order pyramidal and twelve $<111>\{110\}$ bcc slip systems. The bcc slip systems are transformed into the hexagonal coordinate system via the BOR. Hard systems in these colonies are those that intersect the α/β interface. Soft deformation modes are those on which dislocations glide parallel to the α/β interface or have parallel slip planes in both the secondary α and β phases. This crystal plasticity model was also incorporated as a UMAT in ABAQUS [37].

In all cases, the SVEs were loaded in uniaxial tension at room temperature at a quasistatic strain rate of $0.002s^{-1}$. Periodic boundary conditions are applied in all directions to simulate subsurface conditions. The voxellated meshes of these generated microstructures consist of quadrilateral elements with reduced integration (type C3D8R in ABAQUS). For IN100, the number of grains in each simulated SVE ranged between 325-375 grains when each SVE was dimensioned to 0.150 mm along each edge. The distribution of grain volumes normalized by the target average grain volume of $8.0x10^{-6}mm^3$ was fit to a log normal distribution with a mean of -12 and standard deviation of 0.4. This corresponds to a target average cube root grain size of ~0.020mm. There are 24 elements along each edge of the SVE or 13824 elements in all. For IN100, a total of 100 SVEs were generated. The grain averaged FIPs were calculated after the third simulated cycle to allow for shakedown. For Ti-6Al-4V, the number of grains in each generated SVE varied between 325-375. The target volume fraction of the primary α phase was 30%. The standard deviation of the target log-normal grain size distribution for the primary α phase was 25μm and 10μm, respectively. For the $\alpha+\beta$ colonies the mean and standard deviation of the target log-normal grain size distribution was 50μm and 5μm, respectively. These SVEs were all dimensioned 0.400 mm along each edge. There are 26 elements along each edge of the SVE or 17576 elements in all. For Ti-6Al-4V, a total of 100 SVEs were generated. The grain averaged FIPs were calculated after the tenth cycle.

3. Results

3.1. Extreme value marked correlations in IN100

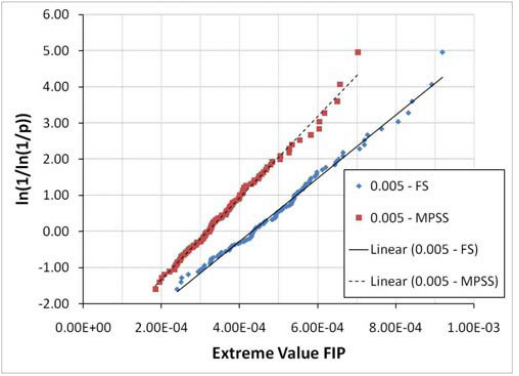

Figure 3 The extreme value grain averaged Fatemi-Socie (FS) and maximum plastic shear strain (MPSS) FIPs calculated over 100 simulated SVEs for IN100 plotted on a Gumbel probability scale.

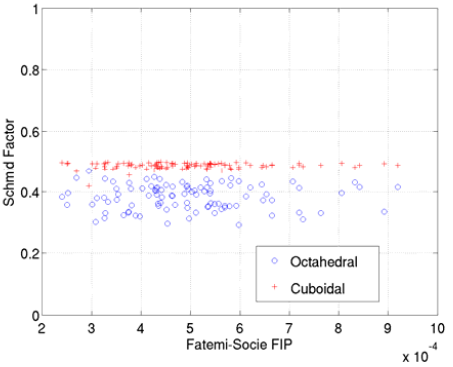

Figure 4 The cross correlations between the Schmid factors for both the octahedral and cube slip systems coincident with the grain average extreme value Fatemi-Socie FIPs in each simulated SVE for IN100.

Figure 3 shows the distributions of the extreme value FS and MPSS FIPs calculated from 100 simulated SVEs of IN100, each cycled three times at 0.5% maximum applied strain under completely reversed loading (i.e. R=-1). This plot is linearized for the Gumbel distribution as outlined in [7]. The parameters of the Gumbel distributions fit via least squares regression to the observed extreme value FIPs are given in
Table 1, where the Gumbel distribution is given as

$$F_{Y_n}(y_n) = \exp\left[-e^{-\alpha_n(y_n-u_n)}\right] \tag{3}$$

The characteristic largest value of the initial variable X is given as u_n, and α_n is an inverse measure of dispersion of the largest value of X. The number of samples of the initial variable X in the set of distributions of X from which Y_n is sampled is n, which for the asymptotic forms listed above is assumed to be very large [39]. The cross correlations between the Schmid factors for both the octahedral and cube slip systems coincident with the grain average extreme value FS FIPs are plotted in Figure 4.

Table 1 Fit Gumbel distribution parameters for the extreme value FIP distributions for IN100.

FIP	α_n	u_n	R^2
FS	8.73×10^{3}	4.31×10^{-4}	0.991
MPSS	1.13×10^{4}	3.18×10^{-4}	0.993

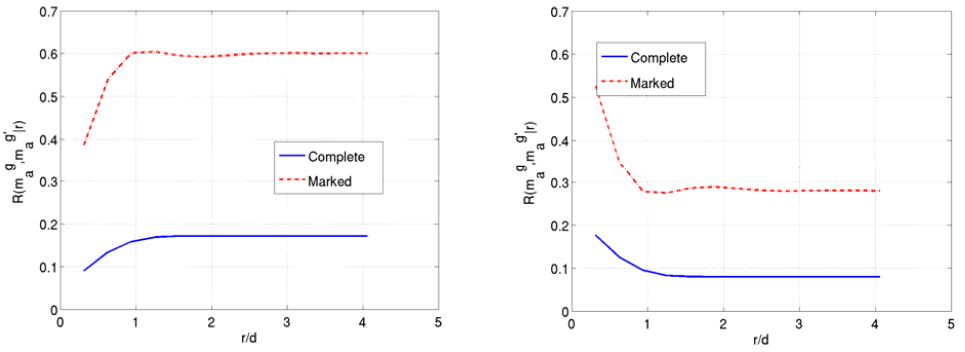

a) b)

Figure 5 Radial correlation functions for the complete microstructure compared with extreme value marked radial correlation functions describing the correlation between the Schmid factors m for a) cube slip between 0.45 and 0.5 and octahedral slip between 0.45 and 0.5 and b) cube slip between 0.45 and 0.5 and cube slip between 0.45 and 0.5.

The extreme value marked correlation functions associated with the extreme value distributions of the FIPs are constructed with the microstructure attribute of the Schmid factor (computed based on the geometry of the slip systems relative to the loading direction). By using the Schmid factor, the probabilities of correlated orientations and misorientations of slip systems are indirectly considered. To construct the extreme value marked correlation functions for the Schmid factor, a range of considered Schmid factors is employed from 0.3 to 0.5 in 0.05 increments. Figure 5 shows the complete radial distribution estimated over the entire ensemble of simulated SVEs and the extreme value marked distribution functions sampled only at the location of the extreme value FIPs for the 100 SVEs cycled at 0.5% strain. The particular correlations plotted in Figure 5 pertain to the Schmid factors for a) cube slip between 0.45 and 0.5 and octahedral slip between 0.45 and 0.5 and b) cube slip between 0.45 and 0.5 and cube slip between 0.45 and 0.5.

3.2. Extreme value marked correlations in Ti-6Al-4V

The extreme value distributions of the FS and MPSS FIPs are given in Figure 6 for the 100 SVEs simulated for Ti-6Al-4V and cycled with a positive mean stress (R=0) to 0.6% maximum strain. The distributions of the extreme value FIPs are plotted on a Gumbel probability scale as describe previously. The estimated distribution parameters for the extreme value Gumbel distribution estimated via linear least squares regression are given in Table 2. The

cross correlations between the Schmid factors for basal, prismatic, pyramidal <*a*>, and pyramidal <*a*+*c*> slip and the grain average extreme value Fatemi-Socie FIP estimated from each of the 100 simulated SVEs of Ti-6Al-4V are plotted in Figure 7.

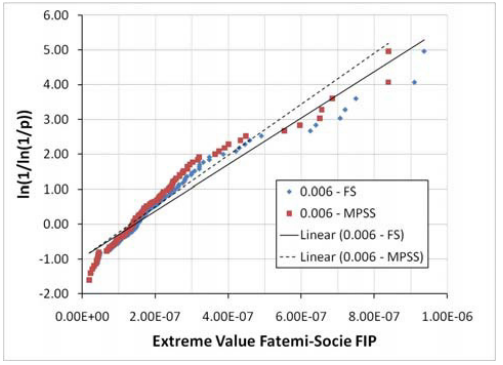

Figure 6 The extreme value grain averaged Fatemi-Socie (FS) and maximum plastic shear strain (MPSS) FIPs calculated over 100 simulated SVEs for Ti-6Al-4V plotted on a Gumbel probability scale.

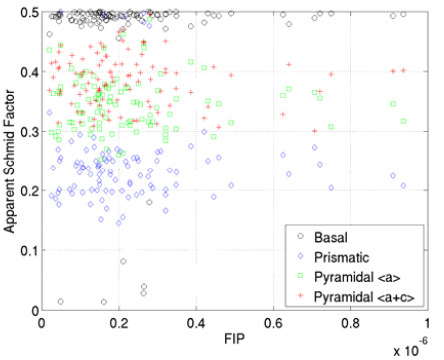

Figure 7 The cross correlations between the Schmid factors for basal, prismatic, pyramidal <a>, and pyramidal <a+c> slip and the grain average extreme value Fatemi-Socie FIP estimated from each of the 100 simulated SVEs of Ti-6Al-4V.

Table 2 Fit Gumbel distribution parameters for the extreme value FIP distributions for Ti-6Al-4V.

FIP	α_n	u_n	$\mathbf{R^2}$
FS	6.68×10^{6}	1.44×10^{-7}	0.934
MPSS	7.33×10^{6}	1.32×10^{-7}	0.934

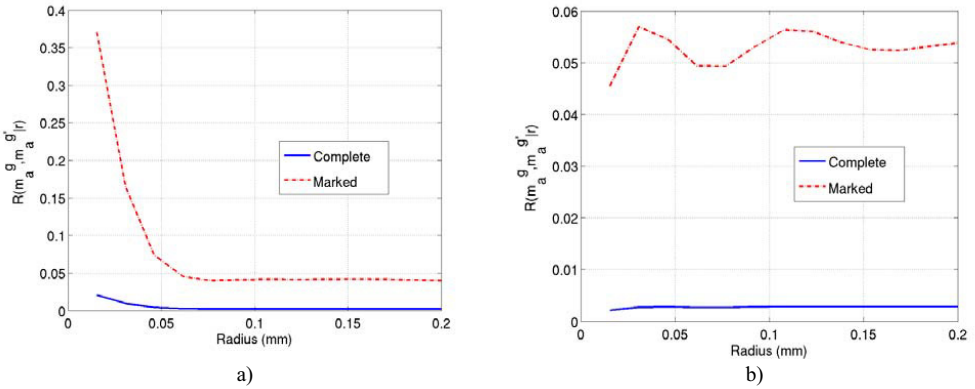

a) b)

Figure 8 Radial correlation functions for the complete microstructure compared with extreme value marked radial correlation functions describing the correlation between Schmid factors for a) basal slip between 0.45 and 0.5 for the primary α phase and basal slip between 0.45 and 0.5 for the primary α phase and b) basal slip between 0.45 and 0.5 for the primary α phase and prismatic slip between 0.45 and 0.5 for the primary α phase.

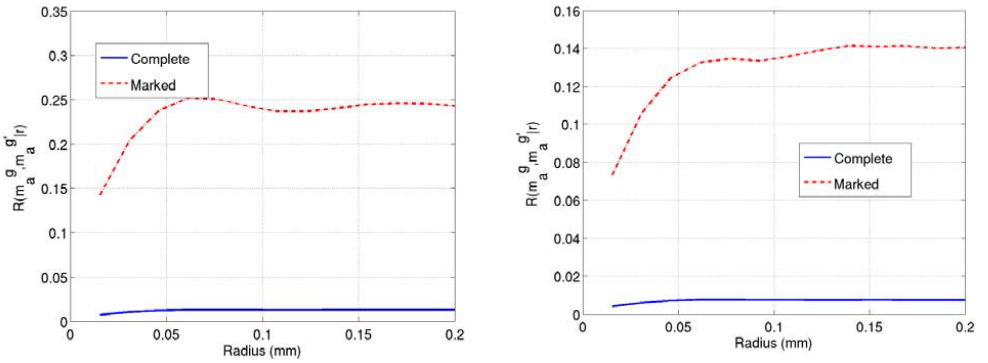

a) b)

Figure 9 Radial correlation functions for the complete microstructure compared with extreme value marked radial correlation functions describing the correlation between Schmid factors for a) basal slip between 0.45 and 0.5 for the primary α phase and $\langle 111 \rangle \{110\}$ bcc slip (transformed into the hexagonal coordinate system via the BOR) between 0.45 and 0.5 for the $\alpha+\beta$ colony phase and, b) basal slip between 0.45 and 0.5 for the primary α phase and pyramidal $\langle a \rangle$ slip between 0.45 and 0.5 for the $\alpha+\beta$ colony phase.

As demonstrated previously for IN100, the extreme value marked correlation functions for Ti-6Al-4V are constructed using the microstructure attribute of the Schmid factor. As shown in Figure 7, grains oriented for easy basal slip were observed to be predominate at locations of the estimated extreme value FIPs. In Figure 8, the radial correlation functions for the complete microstructure compared with extreme value marked radial correlation functions are given describing the correlation between Schmid factors for a) basal slip between 0.45 and 0.5 for the primary α phase and basal slip between 0.45 and 0.5 for the primary α phase and b) basal slip between 0.45 and 0.5 for the primary α phase and prismatic slip between 0.45 and 0.5 for the primary α phase. In Figure 9, the complete and extreme value marked radial distribution functions are given for Schmid factors for a) basal slip between 0.45 and 0.5 for the primary α phase and <111>{110}bcc slip (transformed into the hexagonal coordinate system via the BOR) between 0.45 and 0.5 for the $\alpha+\beta$ colony phase and b) basal slip between 0.45 and 0.5 for the primary α phase and pyramidal $\langle a \rangle$ slip between 0.45 and 0.5 for the $\alpha+\beta$ colony phase.

4. Discussion

The extreme value FIP distributions for the FS and MPSS parameters are similar in character for both IN100 and Ti-6Al-4V. In both material systems, there appears to be less scatter in the extreme value MPSS FIP distribution than then FS FIP distribution. This can be quantified by comparing the values of α_n listed in Tables 1 and 2, recalling that for the Gumbel distribution, α_n is an inverse measure of the dispersion of the largest values of the initial population. In IN100, the grains predicted to exhibit the extreme value response were different between the MPSS and FS FIPs in as many as 10% of the SVEs simulated. There were no grains with the predicted extreme value response in Ti-6Al-4V with the MPSS FIP that were not identically identified by the FS FIP. Although the distributions are similar between the different FIPs, the FS FIP best captures the actual mechanisms of fatigue crack formation based on comparison with previous experimental observations of the local damage processes acting in this class of materials. As shown by McDowell and Berard [40], the FS parameter reflects mixed mode growth of small fatigue cracks. For IN100 and Ti-6Al-4V it is expected to be effective in reflecting combined effects of slip with elevated normal stress to the dominant slip plane(s) arising from intergranular interactions.

In IN100, cube slip is predominate in the locations of predicted extreme value FIPs as evident from Figure 4. In Figure 5, it is evident that there is a much higher probability of finding grains with high Schmid factors (i.e. between 0.45 and 0.5) for cube slip near other grains similarly oriented or octahedral grains with similar high Schmid factors

at the locations of the extreme value FS FIPs than in the overall microstructure. These observations support the results of previous experiments of fatigue in this material system [41]. It is likely that these types of orientation relationships with a high contrast induce additional localize plasticity as the softer phases shed load onto the harder phases during cyclic deformation. Similar high contrast orientation relationships were observed to be important in Ti-6Al-4V.

In Ti-6Al-4V, all of the grains in which the extreme value FIPs are identified were primary α grains. This is expected because slip is much more difficult in the colony grains, particularly at lower strain amplitudes. To consider the orientation of the grains predicted to exhibit the estimated extreme value response, Schmid factors were identified for the primary α HCP slip systems including the basal, prismatic, pyramidal <*a*>, and pyramidal <*a*+*c*> slip systems. In Figure 7, the Schmid factor for each type of slip is compared to the extreme value volume averaged FS FIP for each simulation. In most cases, the grains with the maximum grain averaged FIP are oriented for easy basal slip. Additionally, prismatic slip is also observed but much less often. When the magnitude of the Schmid factor for prismatic slip is high (i.e., close to 0.5), the magnitude of the Schmid factor for pyramidal <*a*> and pyramidal <*a*+*c*> also tends to be fairly high.

The extreme value marked correlation functions constructed from the simulated SVEs for Ti-6Al-4V also indicate that primary α grains oriented with a Schmid factor for basal slip between 0.45 and 0.5 (easy slip) are much more likely to be found at the location of extreme value response than in the overall microstructure (see Figure 8). This agrees with what was found by Bridier *et al.* [15, 16], who investigated fatigue crack formation in Ti-6Al-4V. When considering multiple correlated microstructure attributes, it was much more probable to find a primary *α* grain oriented for easy basal slip or prismatic slip near hard oriented *α*+*β* colonies with high Schmid factors for BOR modified bcc slip or primary α grains with high Schmid factors for pyramidal <*a*+*c*> slip at the locations of the extreme value FS FIP than in the overall microstructure (see Figure 9). The latter previously mentioned correlated orientation relationships were also identified by Gilbert and Piehler [17] and Bantounas *et al.* [42] in Ti-6Al-4V. Various work in *α*+*β* Ti alloys have demonstrated that these types of hard-soft grain combinations can dramatically increase the local stress state which in turn promotes increased plasticity in these regions [26, 43-47]. Thus, similar to that of IN100, these high contrast orientation relationships between softer basal or prismatic grains oriented for easy slip near harder grains oriented for pyramidal or bcc BOR modified slip are predicted to significantly increase the local driving forces for fatigue damage formation.

5. Conclusions

This work has demonstrated the use of a new microstructure-sensitive extreme value probabilistic framework that links the extreme value driving forces for fatigue crack formation in a P/M IN100 and Ti-6Al-4V to the important correlated microstructure attributes that most influence that extreme value response. Specifically, we conclude that:

- Multiple statistical volume elements (SVEs) can be constructed and simulated using appropriate constitutive models to estimate extreme value distributions of key response parameters.
- Cyclic plastic strain based fatigue indicator parameters calculated over nonlocal averaging volumes on the scale of the microstructure attributes important to the mechanisms of fatigue crack formation can be used to identify key microstructure attributes important to the extreme value response.
- In agreement with experiments, the simulations for IN100 predict that cube slip may play an important role in fatigue damage formation particularly when there are multiple grains oriented for cube slip clustered in the same region or clusters of grains oriented for cube slip surrounded by other grains oriented favorable for octahedral slip [14]. Thus, as fatigue crack formation is dominated by the presence of non-metallic inclusions or voids for this particular material system, we expect that given two inclusions of similar character that fatigue cracks will form preferentially near the inclusion that is surrounded by grains or grain clusters unfavorably oriented for octahedral slip.
- In agreement with experiments, the simulations for Ti-6Al-4V predict that primary α grains oriented favorably for basal slip (with a Schmid factor for basal slip between 0.45 and 0.5) have a much higher probability of being associated with the regions of extreme value behavior than in the overall microstructure [15, 16]. Additionally, hard-soft grain interactions between primary α grains oriented favorably for basal slip and primary α grains oriented favorably for pyramidal <*a*+*c*> or *α*+*β* colonies oriented favorably for bcc BOR modified slip are important relative to increased driving forces for fatigue crack formation [17, 42].

Acknowledgements

The authors would like to acknowledge the support of the NSF Center for Computational Materials Design, a joint Penn State-Georgia Tech I/UCRC (NSF IIP 0541678), for development of extreme value HCF and VHCF statistical methods informed by microstructure-sensitive computational models. In addition, Craig P. Przybyla is grateful for the financial support of the Graduate Coop Program at the Air Force Research Laboratory at Wright-Patterson Air Force Base, Dayton, Ohio.

References

[1] S. Suresh, *Fatigue of Materials*, 2nd ed. Cambridge: Cambridge University Press, 1998.
[2] D. L. McDowell, "Basic issues in the mechanics of high cycle metal fatigue," *International Journal of Fracture*, vol. 80, pp. 103-45, 1996.
[3] Y. Murakami, S. Kodama, and S. Konuma, "Quantitative evaluation of defects of non-metallic inclusions on fatigue strength of high strength steels. I: Basic fatigue mechanism and evaluation of correlation between the fatigue fracture stress and the size and location of non-metallic inclusions.," *International Journal of Fatigue*, vol. 11, pp. 291-298, 1989.
[4] S. Beretta and Y. Murakami, "Statistical analysis of defects for fatigue strength prediction and quality control of materials," *Fatigue & Fracture of Engineering Materials & Structures*, vol. 21, pp. 1049-1065, 1998.
[5] H. V. Atkinson and G. Shi, "Characterization of inclusions in clean steels: a review including the statistics of extremes methods," *Progress in Materials Science*, vol. 48, pp. 457-520, 2003.
[6] C. Przybyla, R. Prasannavenkatesan, N. Salajegheh, and D. L. McDowell, "Microstructure-sensitive modeling of high cycle fatigue," *International Journal of Fatigue*, vol. 32, pp. 512-525, 2009.
[7] C. P. Przybyla and D. L. McDowell, "Microstructure-sensitive extreme value probabilities for high cycle fatigue of Ni-base superalloy IN100," *International Journal of Plasticity*, vol. 26, pp. 372-394, 2010.
[8] J. M. Hyzak and I. M. Bernstein, "The effect of defects on the fatigue crack initiation process in 2 p/m super-alloys. 1. Fatigue origins," *Metallurgical Transactions a-Physical Metallurgy and Materials Science*, vol. 13, pp. 33-43, 1982.
[9] M. Goto and D. M. Knowles, "Initiation and propagation behaviour of microcracks in Ni-base superalloy Udimet 720 Li," *Engineering Fracture Mechanics*, vol. 60, pp. 1-18, 1998.
[10] H. T. Pang and P. A. S. Reed, "Fatigue crack initiation and short crack growth in nickel-base turbine disc alloys-the effects of microstructure and operating parameters," *International Journal of Fatigue*, vol. 25, pp. 1089-1099, 2003.
[11] S. K. Jha, M. J. Caton, J. M. Larsen, A. H. Rosenberger, K. Li, and W. J. Porter, "Superimposing mechanisms and their effect on the variability in fatigue lives of a nickel-based superalloy," in *Materials Damage Prognosis*, J. M. Larsen, L. Christodoulou, J. R. Calcaterra, M. L. Dent, M. M. Derriso, W. J. Hardman, J. W. Jones, and S. M. Russ, Eds.: TMS (The Minerals, Metals & Materials Society), 2005.
[12] J. S. Miao, T. M. Pollock, and J. W. Jones, "Crystallographic fatigue crack initiation in nickel-based superalloy Rene 88DT at elevated temperature," *Acta Materialia*, vol. 57, pp. 5964-5974, 2009.
[13] D. Bettge and W. Österle, ""Cube slip" in near-[111] oriented specimens of a single-crystal nickel-base superalloy," *Scripta Materialia*, vol. 40, pp. 389-395, 1999.
[14] K. Li, N. E. Ashbaugh, and A. H. Rosenberger, "Crystallographic Initiation of Nickel-Base Superalloy IN100 at RT and 538°C Under Low Cycle Fatigue Conditions," in *Superalloys 2004*, K. A. Green, T. M. Pollock, H. Harada, T. E. Howson, R. C. Reed, J. J. Schirra, and S. Walston, Eds. Champion, Pennsylvania: The Minerals, Metals & Materials Society (TMS), 2004.
[15] F. Bridier, P. Villechaise, and J. Mendez, "Analyis of slip and crack initiation processes activated by fatigue in a α/β titanium alloy in relation with local crystallographic orientation," presented at 9th International Fatigue Congress, Atlanta, GA, 2006.
[16] F. Bridier, P. Villechaise, and J. Mendez, "Slip and fatigue crack formation processes in an / titanium alloy in relation to crystallographic texture on different scales," *Acta Materialia*, vol. 56, pp. 3951-3962, 2008.
[17] J. L. Gilbert and H. R. Piehler, "On the nature and crystallographic orientation of subsurgace cracks in high cycle fatigue of Ti-6Al-4V," *Metallurgical Transactions A-Physical Metallurgy and Materials Science*, vol. 24, pp. 669-680, 1993.
[18] C. J. Szczepanski, S. K. Jha, J. M. Larsen, and J. W. Jones, "Microstructural influences on very-high-cycle fatigue-crack initiation in Ti-6246," *Metallurgical and Materials Transactions A-Physical Metallurgy and Materials Science*, vol. 39A, pp. 2841-2851, 2008.
[19] S. K. Jha and J. M. Larsen, "Random heterogeneity scales and probabilistic description of the long-lifetime regime of fatigue," in *Fourth International Conference on Very High Cycle Fatigue (VHCF-4)*, J. E. Allison, J. W. Jones, J. M. Larsen, and R. O. Ritchie, Eds. Ann Arbor, Michigan, USA: The Minerals, Metals and Materials Society (TMS), 2007, pp. 385-96.
[20] D. L. McDowell, "Simulation-based strategies for microstructure-sensitive fatigue modeling," *Materials Science and Engineering A*, vol. 468-470, pp. 4-14, 2007.
[21] A. Fatemi and D. F. Socie, "A critical plane approach to multiaxial fatigue damage including out-of-phase loading," *Fatigue and Fracture of Engineering Materials and Structures*, vol. 11, pp. 149-65, 1988.
[22] R. Prasannavenkatesan, J. X. Zhang, D. L. McDowell, G. B. Olson, and H. J. Jou, "3D modeling of subsurface fatigue crack nucleation potency of primary inclusions in heat treated and shot peened martensitic gear steels," *International Journal of Fatigue*, vol. 31, pp. 1176-1189, 2009.
[23] R. Döring, J. Hoffmeyer, T. Seeger, and M. Vormwald, "Short fatigue crack growth under nonproportional multiaxial elastic-plastic strains," *International Journal of Fatigue*, vol. 28, pp. 972-982, 2006.

[24] J. Hoffmeyer, R. Döring, T. Seeger, and M. Vormwald, "Deformation behaviour, short crack growth and fatigue lives under multiaxial nonproportional loading," *International Journal of Fatigue*, vol. 28, pp. 508-520, 2006.
[25] M. Shenoy, J. Zhang, and D. L. McDowell, "Estimating fatigue sensitivity to polycrystalline Ni-base superalloy microstructures using a computational approach," *Fatigue & Fracture of Engineering Materials & Structures*, vol. 30, pp. 889-904, 2007.
[26] F. P. E. Dunne, A. J. Wilkinson, and R. Allen, "Experimental and computational studies of low cycle fatigue crack nucleation in a polycrystal," *International Journal of Plasticity*, vol. 23, pp. 273-295, 2007.
[27] K. O. Findley and A. Saxena, "Low cycle fatigue in Rene 88DT at 650 degrees C: Crack nucleation mechanisms and modeling," *Metallurgical and Materials Transactions A-Physical Metallurgy and Materials Science*, vol. 37A, pp. 1469-1475, 2006.
[28] E. J. Gumbel, *Statistics of Extremes*. New York: Columbia University Press, 1958.
[29] S. Torquato, *Random heterogeneous materials : microstructure and macroscopic properties*. New York: Springer, 2002.
[30] J. Miao, T. M. Pollock, and J. W. Jones, "Fatigue crack initiation in nickel-based superalloy René 88 DT at 593°C," presented at Superalloys, Champion, Pennsylvania, 2008.
[31] A. Brahme, M. H. Alvi, D. Saylor, J. Fridy, and A. D. Rollett, "3D reconstruction of microstructure in a commercial purity aluminum," *Scripta Materialia*, vol. 55, pp. 75-80, 2006.
[32] M. Groeber, S. Ghosh, M. D. Uchic, and D. M. Dimiduk, "A framework for automated analysis and simulation of 3D polycrystalline micro structures. Part 1: Statistical characterization," *Acta Materialia*, vol. 56, pp. 1257-1273, 2008.
[33] M. Groeber, S. Ghosh, M. D. Uchic, and D. M. Dimiduk, "A framework for automated analysis and simulation of 3D polycrystalline micro structures. Part 2: Synthetic structure generation," *Acta Materialia*, vol. 56, pp. 1274-1287, 2008.
[34] "MATLAB," 7.6.0.324 (R2008a) ed: The MathWorks, Inc., 2008.
[35] M. Shenoy, J. Zhang, and D. L. McDowell, "Estimating fatigue sensitivity to polycrystalline Ni-base superalloy microstructures using a computational approach," *Fatigue and Fracture of Engineering Materials and Structures*, vol. 30, pp. 889-904, 2007.
[36] M. Shenoy, Y. Tjiptowidjojo, and D. McDowell, "Microstructure-sensitive modeling of polycrystalline IN 100," *International Journal of Plasticity*, vol. 24, pp. 1694-1730, 2008.
[37] "ABAQUS," 6.7-3 ed. Providence, RI: Simulia, 2007.
[38] F. Bridier, D. L. McDowell, P. Villechaise, and J. Mendez, "Crystal plasticity modeling of slip activity in Ti-6Al-4V under high cycle fatigue loading," 2008.
[39] A. Haldar and S. Mahadevan, *Probability, Reliability and Statistical Methods in Engineering Design*. New York: John Wiley & Sons, Inc., 2000.
[40] D. L. McDowell and J. Y. Berard, "A ΔJ-based approach to biaxial fatigue," *Fatigue and Fracture of Engineering Materials and Structures*, vol. 15, pp. 719-41, 1992.
[41] K. Li, N. E. Ashbaugh, and A. H. Rosenberger, "Crystallographic initiation of nickel-base superalloys IN100 at RT and 538°C under low cycle fatigue conditions," presented at Superalloys, Champion, Pennsylvania, 2004.
[42] I. Bantounas, D. Dye, and T. C. Lindley, "The effect of grain orientation on fracture morphology during high-cycle fatigue of Ti-6Al-4V," *Acta Materialia*, vol. 57, pp. 3584-3595, 2009.
[43] V. Hasija, M. J. Mills, D. S. Joseph, and S. Ghosh, "Deformation and creep modeling in polycrystalline Ti-6Al alloys," *Acta Materialia*, vol. 51, pp. 4533-4549, 2003.
[44] G. Venkataramani, D. Deka, and S. Ghosh, "Crystal plasticity based Fe model for understanding microstructural effects on creep and dwell fatigue in Ti-6242," 2006.
[45] G. Venkatramani, S. Ghosh, and M. Mills, "A size-dependent crystal plasticity finite-element model for creep and load shedding in polycrystalline titanium alloys," *Acta Materialia*, vol. 55, pp. 3971-3986, 2007.
[46] F. P. E. Dunne and D. Rugg, "On the mechanisms of fatigue facet nucleation in titanium alloys," *Fatigue and Fracture of Engineering Materials and Structures*, vol. 31, pp. 949-958, 2008.
[47] F. P. E. Dunne, D. Rugg, and A. Walker, "Lengthscale-dependent, elastically anisotropic, physically-based hcp crystal plasticity: Application to cold-dwell fatigue in Ti alloys," *International Journal of Plasticity*, vol. 23, pp. 1061-1083, 2007.